

Three-Dimensional Bi₅O₇I Photocatalysts for Efficient Removal of NO in Air Under Visible Light

Wei Wang¹ · Yu Huang^{1,2} · Xiaochao Zhang³ · Jun-ji Cao^{1,2} · Wingkei Ho^{1,4} · Shun Cheng Lee⁵

Received: 25 December 2016 / Revised: 11 February 2017 / Accepted: 21 February 2017 / Published online: 23 March 2017
© Institute of Earth Environment, Chinese Academy Sciences 2017

Abstract In this study, we report a flower-like Bi₅O₇I photocatalyst with a 41% gaseous nitride oxide (NO) removal efficiency under visible light through the in situ thermal treatment of the hierarchical architecture BiOI synthesized using a facile hydrothermal process. The UV–Vis diffuse reflectance spectroscopy and photocurrent experiments showed that the absorption band edge and photo-induced electron–hole pairs separation efficiency of Bi₅O₇I were negative than that of BiOI, whereas the as-prepared Bi₅O₇I exhibited excellent and stable visible light photocatalytic performance for NO removal as compared with original BiOI and P25. The results of electron spin resonance spectroscopy and density functional theory calculations suggested that the prominent visible light photocatalytic activity of obtained Bi₅O₇I has been attributed to the proper electron band structure which oxidizes the O₂ molecule to ·OH radicals with two electrons in the conduction band.

Electronic supplementary material The online version of this article (doi:10.1007/s41810-017-0003-3) contains supplementary material, which is available to authorized users.

✉ Yu Huang
huangyu@ieecas.cn

- ¹ Key Laboratory of Aerosol Chemistry & Physics, Institute of Earth Environment, Chinese Academy of Sciences, Xi'an 710061, China
- ² State Key Laboratory of Loess and Quaternary Geology (SKLLQG), Institute of Earth Environment, Chinese Academy of Sciences, Xi'an 710061, China
- ³ College of Chemistry and Chemical Engineering, Taiyuan University of Technology, Taiyuan 030024, China
- ⁴ Department of Science and Environmental Studies, The Education University of Hong Kong, Hong Kong, China
- ⁵ Department of Civil and Environmental Engineering, The Hong Kong Polytechnic University, Hung Hom, Hong Kong

Keywords NO_x removal · Photocatalysis · Bi₅O₇I · Bismuth compounds

1 Introduction

Nitrogen oxides (NO_x), which are important precursors of secondary fine particulate matters, have crucial contributions to the formation of the haze problem (Huang et al. 2014). Hence, NO_x abatement is a crucial issue that must be addressed. In recent years, photocatalysis has been emerged as an intriguing technology for various air pollutants destruction since the initial study by Frank and Bard (1977). The merit of this technology is the use of solar energy to achieve the efficient decomposition of recalcitrant substances in mild conditions. The complex photocatalytic reaction process can be simplified into three steps: generation/separation, transfer, and consumption of photo-generated carriers (Huang et al. 2016). That is, the photocatalytic activity of photocatalysts has been related to its photo-absorption, photo-induced carrier separation, and redox ability. Therefore, the electronic structure of photocatalysts, which primarily determines its physical and chemical properties, has been extensively studied to guide the exploration of visible light-driven photocatalysts.

To date, TiO₂-based materials are the most mature photocatalysts because of their stability, as well as their non-toxic and easily accessible properties (Chen et al. 2015; Deng et al. 2002; Gomathi and Kavitha 2014; Tada et al. 2009). Apart from TiO₂-based semiconductors, non-TiO₂-based materials also become a research hotspot in the field of contamination control (Brahimi et al. 2008; Jinlin et al. 2014; Liu et al. 2014; Marin et al. 2012; Martinez Suarez et al. 2015; Wang et al. 2015; Zhang and Zhu 2012; Zhang et al. 2016; Zhao et al. 2015). Among these materials, bismuth oxide compounds are

prominent due to their special layer structure, which is beneficial to electron transfer in the interlayer Liu et al. (2010). Besides, Bi 6s and O 2p orbitals can form a new valence band in a row above the original position through orbital hybridization, thereby effectively reducing the band gap and producing visible light absorption (Martinez Suarez et al. 2015). Especially, bismuth oxyhalides, as a typical layer-structured photocatalytic materials, have been successfully prepared and applied in the water purification of organic pollutants (Ahern et al. 2015; Henle et al. 2007; Sun et al. 2015; Wang et al. 2011). At the same time, its application in the field of air pollution control is quite rare (Ai et al. 2009; Zhang et al. 2013; Zhang et al. 2016).

In this study, we present a flower-like Bi₅O₇I material through a facile hydrothermal process followed by thermal treatment, and thereafter used to remove NO at ppb levels under visible light irradiation. The photocatalytic activity of Bi₅O₇I on NO removal was considerably higher than that of BiOI because of the proper band energy structure, despite of which the optical absorption ability and photo-excited charge carriers separation efficiency have become weak. Theoretical evaluation was also undertaken to explore the mechanism regarding to the enhancement of photocatalytic activity.

2 Experimental

2.1 General Information

All chemicals used in this study were of analytical grade and used without further purification. Bi(NO₃)₃·5H₂O was purchased from Sigma-Aldrich. Potassium iodide (KI) and ethanol were bought from Sinopharm Chemical Reagent Co., Ltd. (China). Distilled water (Milli Q water) was used throughout all the experiments.

2.2 Sample Preparation

The Bi₅O₇I photocatalyst was synthesized using the hydrothermal method followed by a simple calcination. In a typical procedure, 2 mmol of Bi(NO₃)₃·5H₂O was completely dissolved in 2 mL glacial acetic acid, and 20 mL deionized water was added to become the Bi(NO₃)₃·5H₂O solution. Thereafter, the Bi(NO₃)₃·5H₂O solution was added to the KI solution, which was composed of 2 mmol KI and 15 mL of deionized water, drop by drop with stirring. After agitating vigorously for 30 min at room temperature, the formed suspension liquid was transferred to a 50 mL Teflon-lined stainless steel autoclave and heated at 140 °C for 24 h. When the autoclave was cooled naturally to room temperature, the carmine BiOI sample was collected, washed thrice with deionized water and absolute ethanol, and dried overnight at 70 °C. To obtain the Bi₅O₇I product, the as-prepared BiOI sample was further calcined at 450 °C for 3 h.

2.3 Characterization

The powder XRD patterns were obtained using a PANalytical X' Pert PRO X-ray diffractometer at 40 kV and 40 mA with Cu K α radiation ($\lambda = 1.5406 \text{ \AA}$). TG-DSC was performed using a Simultaneous Thermal Analysis instrument STA 449F5 from room temperature to 800 °C under air flow (30 mL/min). A few SEM images were obtained using a JSM-6700 field-emission scanning electron microscope. Several TEM images were recorded on a JEOL JEM-2010 electron microscope operated at an accelerating voltage of 200 kV. Imaging samples were prepared by ultrasonically dispersing limited samples in absolute ethanol, and the dispersion was dropped on carbon-coated copper grids. The BET surface area was determined using a nitrogen adsorption apparatus Gemini 2390. The UV–Vis diffuse reflectance spectroscopy (DRS) spectra were recorded at room temperature using an Agilent Cary-100 UV–Vis spectrophotometer equipped with an integrated sphere. The DMPO-ESR spin-trapping was performed using a fluorescence spectrometer (FLsp920, Edinburgh Instruments), and the sample for the ESR measurement was prepared by mixing the as-prepared samples with 50 mM DMPO (5,5'-dimethyl-1-pyrroline *N*-oxide) solution for the detection of free radicals.

2.4 Photoelectrochemical Measurements

The photoelectrochemical properties of the as-prepared samples were evaluated using a Parstat4000 electrochemical workstation (Princeton, USA) in a conventional three-electrode cell, in which a platinum plate and a Ag/AgCl electrode were used as a counter electrode and a reference electrode, respectively. To fabricate the working electrode, 20 mg Bi₅O₇I or BiOI was dispersed into a 4 mL 1 wt% Nafion ethanol solution to obtain a homogeneous suspension through bath sonication. Thereafter, the BiOI or Bi₅O₇I films were modified on the fluorine-doped tin oxide (FTO) conducting glass by dip coating and dried at room temperature. The current–time curves were measured at 0.0 V versus Ag/AgCl in 0.1 mol L⁻¹ Na₂SO₄ at ambient temperature under a 300 W Xe arc lamp.

2.5 Photocatalytic NO_x Removal Experiments

Batch experiments were performed in a continuous flow reactor at room temperature to investigate the photocatalytic performance of the prepared photocatalysts for the removal of NO in air. The rectangular reactor, which was made of stainless steel, was covered with quartz glass; the volume of the reactor was 4.5 L (10 cm × 30 cm × 15 cm (H × L × W)). A 300 W commercial Xenon lamp ($\lambda > 290 \text{ nm}$) with and without a 420 nm cutoff filter was used to provide the simulated solar and visible light irradiation, respectively. The

sample dish, which was prepared by mixing a 50 mg catalyst with deionized water and evaporating at 70 °C to form a uniform coating layer, was placed in the middle of the reactor. The lamp was vertically placed outside the reactor above the sample dish. The NO gas was acquired from a compressed gas cylinder at a concentration of 48 ppm NO with a traceable National Institute of Standards and Technology (NIST) standard. The initial concentration of NO was diluted to approximately 400 ppb by the air stream supplied by a zero air generator (Sabio model 1001), and the flow rate was controlled at 3 L/min. The lamp was turned on after the adsorption–desorption equilibrium was achieved. The NO concentration was continuously recorded by a chemiluminescence NO_x analyzer (EC 9841 series NO_x) with a sampling rate of 0.6 L/min. The whole measurement was conducted at ambient conditions with the relative humidity (RH) of 30 ± 5%. The removal rate (%) of NO was evaluated with the ratio of the NO concentration in the feeding stream and that in the outlet stream: η (%) = C/C_0 . A control experiment with or without light was performed, thereby showing that the reaction of NO with air was negligible in the absence of photocatalysts. In addition, different kinds of scavengers were utilized to evaluate the roles of the reactive species during the photocatalytic process, including potassium iodide (KI) for h⁺, K₂Cr₂O₇ for e⁻ and tert-butyl alcohol (TBA) for hydroxyl radical (·OH). During preparing the sample dish, the specific scavenger was added into the suspension containing photocatalyst to obtain uniform sample coating layer through the evaporation of water.

2.6 Computational Details

In this work, the first-principles calculation was performed using the well-tested Cambridge Serial Total Energy Package (CASTEP) code based on density functional theory (DFT), and the exchange–correlation functional was described with the generalized gradient approximation (GGA) within the scheme of Perdew–Burke–Ernzerhof (PBE). For relative investigations on the electronic structures and ground-state properties of BiOI and Bi₅O₇I samples, the valence electronic configurations were Bi-6s²6p, O-2s²2p⁴- and I-5s²5p⁵ states. The Vanderbilt-type ultrasoft pseudopotentials was used with a cut off energy of 340 eV. The Brillouin zone integrations were approximated using a 4 × 4 × 2 *k*-point grid sampling scheme of Monkhorst–Pack. To further obtain reasonable calculations, the geometrical structure and lattice parameters of BiOI and Bi₅O₇I crystals are optimized by an iterative process, in which the maximum root-mean-square convergent tolerance, force convergence thresholds, and stress tolerances were less than 1 × 10⁻⁶ eV/atom, 0.1 eV/nm and 0.1 GPa, respectively. Then, the electronic band structures of the optimized BiOI and Bi₅O₇I crystals were calculated and discussed.

3 Results and Discussion

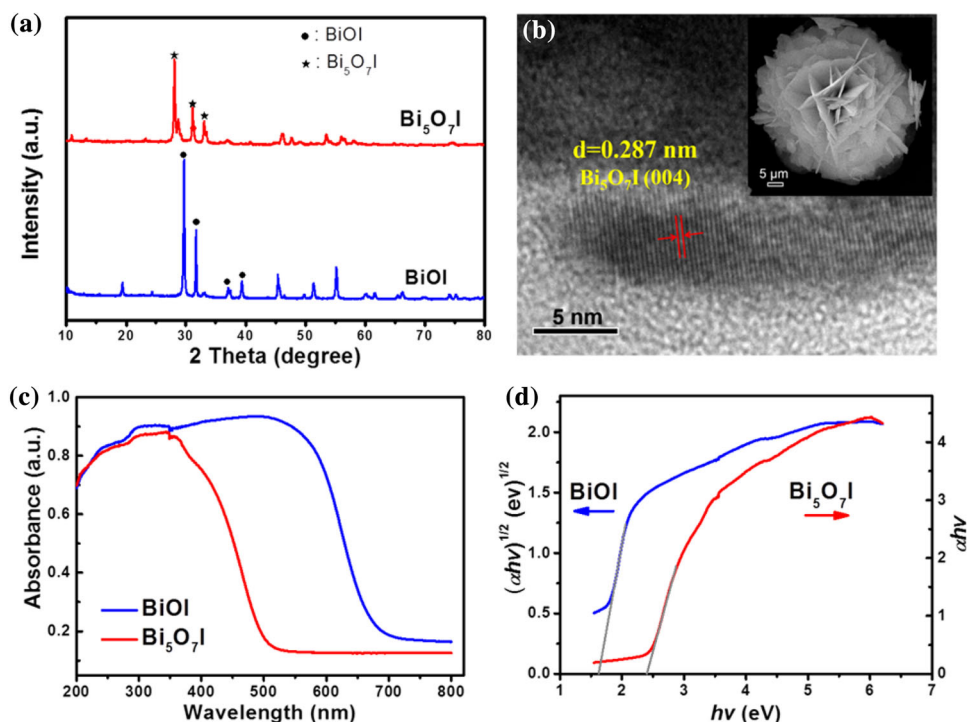
3.1 Material Characterization

Figure S1 illustrates the synthesis procedure of Bi₅O₇I. Bi₅O₇I was obtained via a facile hydrothermal procedure followed by an *in situ* post-calcination treatment of the BiOI precursor. We can expect to obtain the Bi₅O₇I phases by precise control of the calcination time and temperature based on the thermal decomposition profile of BiOI (Fig. S2). X-Ray powder Diffraction (XRD) (Fig. 1a) reveals that the hydrothermally synthesized precursor could be indexed to a pure tetragonal phase of the bismuth oxide iodide (BiOI) (JCPDS file No. 73-2062). After the calcination of BiOI precursor at 450 °C for 3 h, the diffraction peaks in the XRD pattern of these powders can be indexed to the orthorhombic Bi₅O₇I (JCPDS file No. 40-548). No other impurity phases were observed, thereby indicating the good phase purity of the products. Therefore, the orthorhombic Bi₅O₇I have been successfully synthesized through the calcination of the BiOI precursor at 450 °C for 3 h. Moreover, the decomposition of the precursor at 450 °C for 1 h resulted in a powder, of which the XRD peaks located at 29.6° exhibited a slight low degree shift to 28.9° (Fig. S3). Thus, BiOI has been converted segmentally to Bi₅O₇I, and the generated Bi₅O₇I calcinate and BiOI precursor spread to the crystal lattice of the other side to form a solid solution during the calcination process through the miscibility effect. As the calcination time prolonging, the low degree shift continues until typical peaks corresponding to the orthorhombic Bi₅O₇I (120) at 28.2° (Fig. S3).

The morphologies of the samples were characterized via SEM. The SEM images (see Fig. S4a) show that the BiOI precursor is a flower-like hierarchical architecture because it comprised various well-defined nanoplates. After calcination at 450 °C for 3 h, the flower-like hierarchical architecture of Bi₅O₇I shows insignificant changes, and the surface of the nanoplate of Bi₅O₇I comprises many small holes (Fig. S4b). Meanwhile, the lattice spacing of Bi₅O₇I is 0.287 nm, which can match the spacing of the (004) crystal plane of Bi₅O₇I (Fig. 1b). The BET surface area of Bi₅O₇I is determined to be 4.78 m²/g, which is better than that of BiOI (3.53 m²/g). The increase in the surface area of Bi₅O₇I is associated with the morphological change that is caused by the release of I₂: 5 BiOI + O₂ → Bi₅O₇I + 2 I₂ (see Figs. S2 and S4b).

The UV–Vis diffuse reflectance absorption spectroscopy was performed to determine the optical properties of the as-prepared samples (Fig. 1c). Figure 1c shows that the absorption range of the Bi₅O₇I sample occurs with the blue shift from 700 nm to approximately 500 nm compared with the BiOI precursor. Moreover, Bi₅O₇I displays a similarly strong absorption in the UV-light region. In addition, Bi₅O₇I is a direct semiconductor, whereas BiOI is an indirect one. Plots of $\alpha h\nu$ or $(\alpha h\nu)^{1/2}$ versus the energy of the

Fig. 1 **a** XRD patterns of the as-prepared samples. **b** SEM and HRTEM images of the $\text{Bi}_5\text{O}_7\text{I}$ calcinate. **c** UV–Vis diffuse reflectance spectra of the as-prepared samples. **d** Plots of $(\alpha h\nu)^{1/2}$ or $\alpha h\nu$ versus energy $h\nu$ for BiOI and $\text{Bi}_5\text{O}_7\text{I}$, respectively



absorbed light provide the bandgap of semiconductors (Fig. 1d), respectively. The bandgap energy of BiOI estimated from the intercept of the tangent to the plot is 1.60 eV. Compared with the pristine BiOI, the obtained $\text{Bi}_5\text{O}_7\text{I}$ has obvious light absorption below 500 nm, and the onset of $\text{Bi}_5\text{O}_7\text{I}$ corresponds to a band gap of 2.36 eV.

3.2 Photocatalytic Performances on NO Removal

The photocatalytic activities of the as-prepared photocatalysts were evaluated in terms of gaseous NO removal, and the photocatalytic powders were measured using FT-IR. Figure 2a shows the variations of the NO concentration versus irradiation time in the presence of the as-calcined samples under artificial visible light irradiation with the commercial P25 photocatalyst as a reference. The NO removal rates were ignorable without the presence of photocatalyst under simulated visible light irradiation. Under visible light irradiation, the $\text{Bi}_5\text{O}_7\text{I}$ calcinate could remove 41.6% of NO in 30 min, whereas only 5.3% of NO is removed with the original BiOI (Fig. 2a). This comparison suggests that the obtained $\text{Bi}_5\text{O}_7\text{I}$ could efficiently enhance the photocatalytic performance compared with both the BiOI precursor and commercial P25 photocatalyst. Figure S5 shows that the NO removal trend under solar light is consistent with that under visible light irradiation in the same system.

3.3 Mechanism on Photocatalytic Activity Enhancement and NO Degradation

The photo-responses of the BiOI and $\text{Bi}_5\text{O}_7\text{I}$ electrodes on on–off cycles were investigated to determine the separation efficiency of the photo-induced electron–hole pairs. As shown in Fig. 3a, the photocurrent intensity generated by the BiOI electrode decays rapidly and drastically as the time goes on, while that generated by $\text{Bi}_5\text{O}_7\text{I}$ electrode keeps good stability. And the result shows that the photocurrent intensity generated by the BiOI electrode is approximately 1.5 times of that generated by the $\text{Bi}_5\text{O}_7\text{I}$ electrode under simulated solar light irradiation, indicating that stable trend of photo-induced carrier separation process comes along with partially negative separation rate of photo-generated electron–hole pairs *via* the calcination treatment of the BiOI precursor.

The photocatalytic reaction is described as the process of the generation, transfer, and consumption of the photo-generated carriers under light illumination. Photo-absorption, separation of photo-induced electron–hole pairs, and energy band structure play important roles in photocatalytic reaction process. The preceding results reveal that the formation of the $\text{Bi}_5\text{O}_7\text{I}$ can enhance their photocatalytic activities under either solar or visible light irradiation, even though the treatment narrows their light absorption region, and decrease the separation efficiency of the photo-induced electron–hole pairs (Figs. 1c and 3a). Thereafter, it is hypothesized that it may be a proper energy band character, thereby

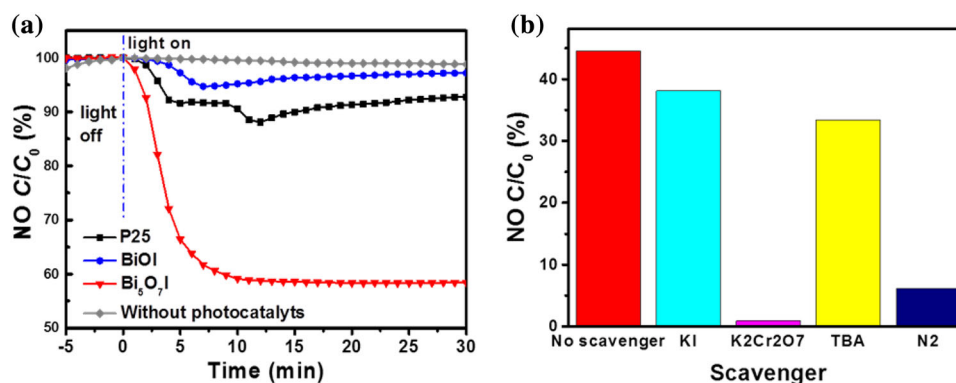


Fig. 2 **a** Photocatalytic activities of the as-prepared samples under visible light for the NO removal. **b** The effect of addition of quenchers on the photocatalytic activity of Bi₅O₇I under solar light irradiation for NO

providing the Bi₅O₇I calcinate substantially effective photocatalytic activity for the removal of NO compared with the original BiOI.

The electronic band structures of the resulting samples were investigated through density functional theory (DFT) calculations. The DFT results show that the valence band maximum (VBM) and conduction band minimum (CBM) of BiOI and Bi₅O₇I were 2.51/0.91 and 2.91/0.55 eV, respectively. Figure 5a shows the energy band structure of the original BiOI and obtained Bi₅O₇I based on the preceding data. Both BiOI precursor and calcinated Bi₅O₇I have efficient visible light spectral absorption because of their proper band gaps. The valence band potential of either Bi₅O₇I (above 2.91 V vs. normal hydrogen electrode (NHE)) or BiOI (above 2.51 V vs. normal hydrogen electrode (NHE)) is more positive than the redox potential of OH⁻/·OH (1.99 V). Therefore, the photo-induced holes at the valence band of both can oxidize OH⁻ into ·OH radicals. Furthermore, given the redox potential of O₂/H₂O₂ is 0.695 V, the photo-excited electrons of Bi₅O₇I can reduce O₂ to H₂O₂ instead of reducing O₂ into O₂⁻. This can be attributed to the conduction band potential of Bi₅O₇I being more positive than that of the redox potential of O₂/O₂⁻. The formed H₂O₂ would be further transformed into ·OH by capturing an electron. Conversely, the BiOI electrons have low redox potential because of its positive conduction band potential.

The DMPO-ESR spin-trapping spectra of the as-prepared samples were measured to investigate the major active species that drive the obtained Bi₅O₇I to possess such an exceptionally different light activity compared with the BiOI precursor. Figure 3b shows DMPO-ESR spin-trapping spectra of BiOI and Bi₅O₇I for the detection of the hydroxyl radicals (·OH) in aqueous solution and (·O₂⁻) superoxide radicals in methanol under UV light irradiation. Under UV light irradiation, the ·OH radicals are detected (Thornalley et al. 1983) for all the as-prepared samples. The results show that

removal. Quenchers: potassium iodide (KI, a hole scavenger), potassium bichromate (K₂Cr₂O₇, a e⁻ scavenger), tert-butyl alcohol (TBA, a ·OH radical scavenger), and no scavenger (N₂ as O₂ substitution)

the signal of the ·OH radicals for Bi₅O₇I is stronger than that of the BiOI precursor after turning on the UV light for 2 min. A slight signal of CH₃OH for both Bi₅O₇I and BiOI is also apparent, whereas no similar signal is observed for the ·O₂⁻ radicals Dillon et al. (1996). These results indicate that the ·OH radicals are major reactive oxidation species during the photocatalysis removal process of NO_x under the as-prepared photocatalysts. Also, Bi₅O₇I could produce additional ·OH radicals, which is responsible for its enhanced photocatalytic activity and oxidation ability. Furthermore, a trapping experiment with different quenchers (e.g., potassium bichromate (K₂Cr₂O₇, a e⁻ scavenger), potassium iodide (KI, a hole scavenger), and tert-butyl alcohol (TBA, a ·OH radical scavenger)) under solar light irradiation of Bi₅O₇I for NO removal was performed to probe the possible factors that affected the ·OH intensity of Bi₅O₇I (Fig. 2b). The results show that the addition of a 1% KI or TBA causes the segmental deactivation of Bi₅O₇I, and the existence of 1% K₂Cr₂O₇ causes nearly the complete inactivation of Bi₅O₇I. Replacing O₂ with N₂ to act as a balance gas resulted in the NO removal efficiency of only 5% (Fig. 2b), which indicate that the ·OH radicals resulting from the reduction of O₂ by e⁻ are major reactive oxidation species during the photocatalytic removal process of NO_x over Bi₅O₇I. Conversely, the ·OH radicals originating from the valence band is a minor factor during the entire photocatalytic process.

The band structures for BiOI and Bi₅O₇I supercells with 102 atoms were calculated by DFT method to further confirm the energy level advantage of Bi₅O₇I for use in the photocatalytic NO removal process. Figure 4 shows that BiOI has an indirect band gap behavior, whereas Bi₅O₇I has the direct band gap characteristics. Thus, Bi₅O₇I has a lower electron transition efficiency and higher carrier recombination efficiency than those of BiOI Long et al. (2009) (Fig. 3a). Besides, the possible electron transition energy of BiOI from VBM to the lowest unoccupied molecular orbital (LUMO)

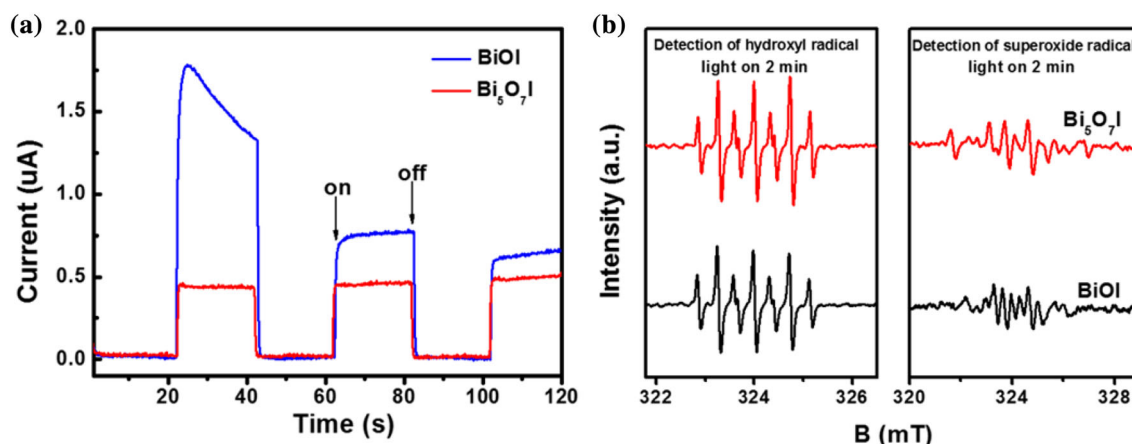


Fig. 3 **a** Photocurrent plot of the as-calcinated sample photoelectrodes. **b** DMPO-ESR spin-trapping spectra of BiOI and Bi₅O₇I for the detection of the hydroxyl radicals ($\cdot\text{OH}$) in aqueous solution and ($\cdot\text{O}_2^-$) superoxide radicals in methanol under UV light irradiation

is approximately 1.453 eV, which is similar but underestimated compared with the experimental value of 1.60 eV due to the limitation of DFT (Fig. 1d). By contrast, for the Bi₅O₇I model, the calculated band energy is 2.272 eV, which is slightly narrower than that determined by UV-DRS as BiOI (Figs. 1d and 4b). This result means that the blue-shift would be observed when the original BiOI is replaced by the obtained Bi₅O₇I (Fig. 1c). Figure 4c, d show that the partial and total density of states of BiOI and Bi₅O₇I. Although the CBM of both BiOI and Bi₅O₇I mainly comprises Bi 6p orbits, the P2 peak of Bi₅O₇I is slightly more negative than that of BiOI. Thus, the redox potential of Bi 6s is caused by Bi₅O₇I being stronger than that located at BiOI. Moreover, the VBM of BiOI comprises Bi 6s and I 5p orbits, and the VBM of Bi₅O₇I is significantly dispersed by O 2p orbits. Thus, the photo-induced holes have a small effective mass. The foregoing observations can explain that BiOI has a small band gap of approximately 1.60 eV and high separation efficiency of the photocatalytic carriers, but Bi₅O₇I has a high photocatalytic activity.

On the basis of the preceding experimental and theoretical calculation results, the possible solar light photocatalytic mechanism of the BOI-calcined for the removal of NO could be explained as follows (Fig. 5a). Under either an entire solar or visible light irradiation, BiOI and Bi₅O₇I are excited and produce photo-generated electron–hole pairs. BiOI has a low probability of photo-generated carriers recombination because the original BiOI shows significant photocurrent intensity compared with the Bi₅O₇I calcinate (Figs. 3a and 4), thereby resulting in an enhanced carrier participation in the subsequent target removal reaction compared with Bi₅O₇I. After the separation of the photo-induced carriers, the photo-excited electrons and holes of Bi₅O₇I indirectly reduce O₂ or H₂O into the active species $\cdot\text{OH}$ by capturing one or two electrons. While just the photo-induced holes at the valence band

of BiOI oxidize OH[−] into the active species ($\cdot\text{OH}$) that are responsible for the removal of gaseous NO. Thereafter, the resulting active species $\cdot\text{OH}$ oxidize NO to the final HNO₃ products (Fig. 5a). Bi₅O₇I produces numerous $\cdot\text{OH}$ radicals because the signal of the $\cdot\text{OH}$ radicals for Bi₅O₇I is evidently stronger than that of the BiOI precursor; Thus, Bi₅O₇I produces many $\cdot\text{OH}$ radicals and has a better removal capacity than the original BiOI (see Figs. 2b and S5).

Multiple runs of photo degradation experiments and long-term tests suggest that Bi₅O₇I is relatively stable and cannot be easily photo-corroded during the photocatalytic process (Fig. S6), in accordance with the stable trend reflected by the photocurrent plot (Fig. 2a). The stability of Bi₅O₇I is further confirmed by the FI-TR spectra of Bi₅O₇I before and after recycling irradiation (see Fig. 5b). A characteristic band group in FT-IR at 504 cm^{−1} (i.e., symmetrical A_{2u}-type vibrations of the Bi–O bond) Chang et al. (2013) is observed for the fresh and tested photocatalysts. Meanwhile, the represented peaks located at 1380 and 843 cm^{−1} can be attributed to the reaction intermediates, and the reaction products during the photocatalytic oxidation of NO (e.g., NO₂[−] and NO₃[−]) can be observed. We further note that the reaction intensifies with the recycling times.

4 Conclusion

In summary, a flower-like Bi₅O₇I calcinate, which could considerably enhance the photocatalytic capability on the removal of NO under visible light irradiation and keep relatively excellent photocatalytic efficiency after long-term irradiation was achieved via the hydrothermal method followed by the *in situ* calcination of the BiOI precursor. This enhanced photocatalytic capability benefited from the suitable electron band structure which gives Bi₅O₇I good redox

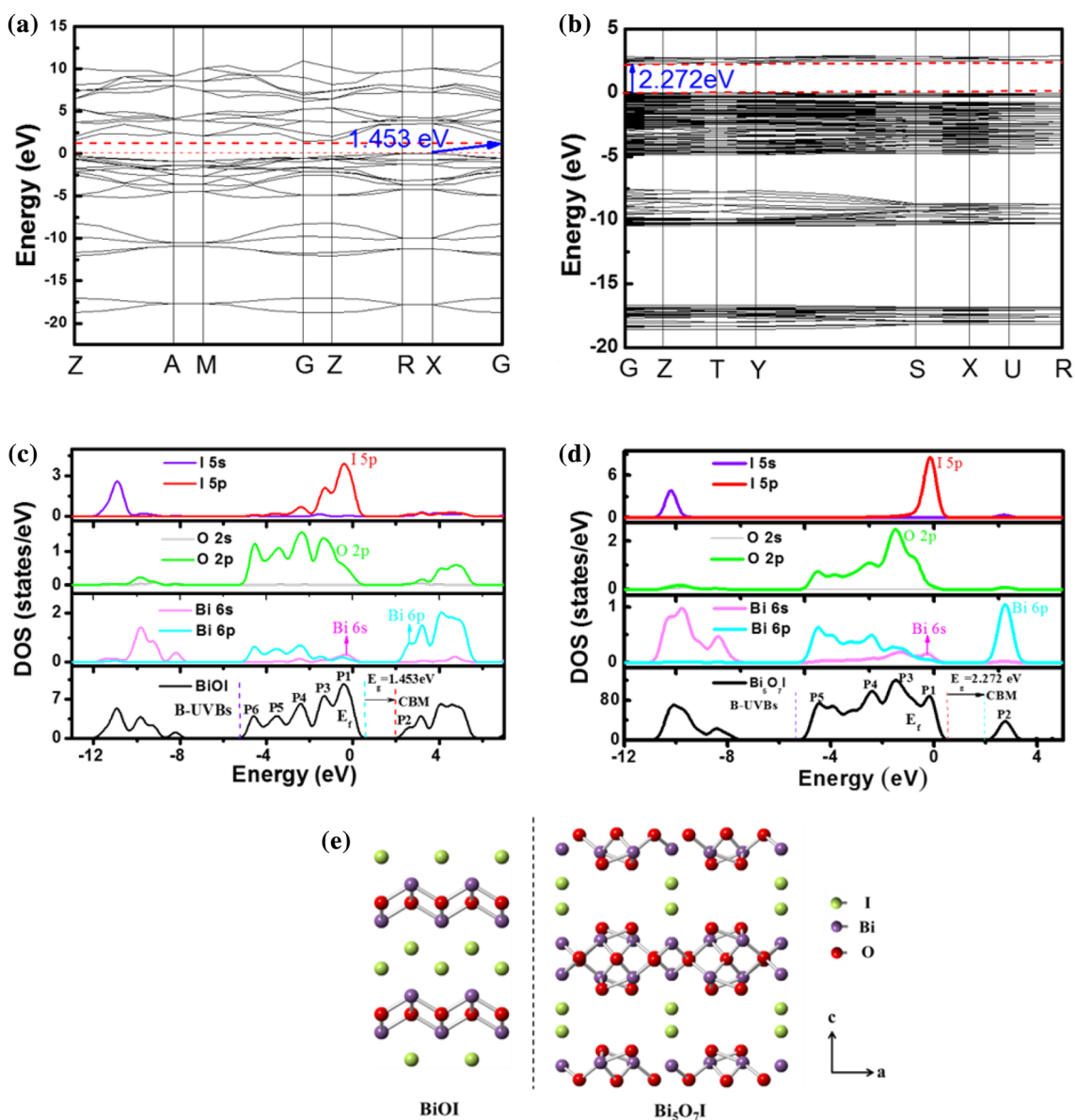
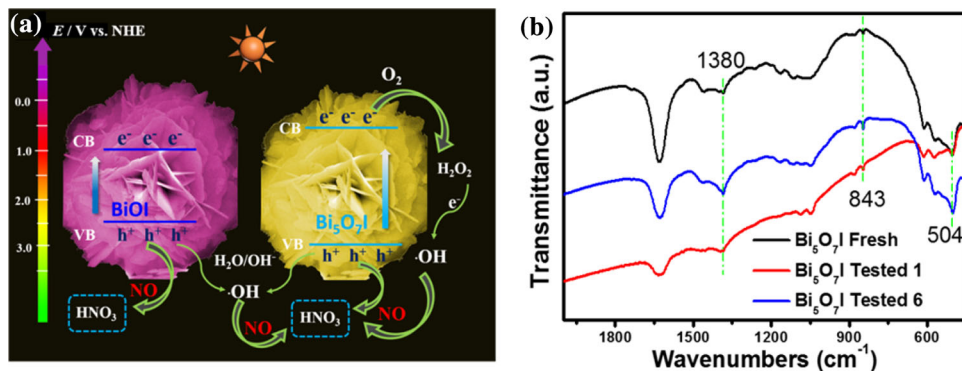


Fig. 4 Calculated band structure of **a** BiOI and **b** Bi₅O₇I. The calculated TDOS and PDOS corresponding to **c** BiOI and **d** Bi₅O₇I. The zero energy line represents the Fermi level. **e** Schematic layered structure of BiOI and Bi₅O₇I

Fig. 5 a Schematic diagram of the energy bands of BiOI and Bi₅O₇I, as well as the reactions under the simulated solar light ($\lambda > 290$ nm) irradiation during the photocatalytic process. **b** FT-IR spectra of the fresh and tested Bi₅O₇I



ability and dependent on the presence of $\cdot\text{OH}$ radicals. It is expected that $\text{Bi}_5\text{O}_7\text{I}$ calcinate can have promising applications for air purification.

Acknowledgements This research was financially supported by the National Science Foundation of China (41401567, 41573138) and the “Strategic Priority Research Program” of the Chinese Academy of Sciences (Grant No. XDB05000000). Yu Huang is also supported by the “Hundred Talent Program” of the Chinese Academy of Sciences.

References

- Ahern JC, Fairchild R, Thomas JS, Carr J, Patterson HH (2015) Characterization of BiOX compounds as photocatalysts for the degradation of pharmaceuticals in water. *Appl Catal B* 179:229–238. doi:10.1016/j.apcatb.2015.04.025
- Ai Z, Ho W, Lee S, Zhang L (2009) Efficient photocatalytic removal of NO in indoor air with hierarchical bismuth oxybromide nanoplate microspheres under visible light. *Environ Sci Technol* 43:4143–4150
- Brahimi R, Bessekhouad Y, Bouguelia A, Trari M (2008) Improvement of eosin visible light degradation using PbS-sensitized TiO₂. *J Photochem Photobiol A* 194:173–180
- Chang C, Zhu L, Fu Y, Chu X (2013) Highly active Bi/BiOI composite synthesized by one-step reaction and its capacity to degrade bisphenol A under simulated solar light irradiation. *Chem Eng J* 233:305–314
- Chen X, Liu L, Huang F (2015) Black titanium dioxide (TiO₂) nanomaterials. *Chem Soc Rev* 44:1861–1885. doi:10.1039/C4CS00330F
- Deng X, Yue Y, Zi G (2002) Gas-phase photo-oxidation of organic compounds over nanosized TiO₂ photocatalysts by various preparations. *Appl Catal B* 39:135–147
- Dillon J, Gaillard ER, Bilski P, Chignell CF, Reszka KJ (1996) The Photochemistry of the retinoids as studied by steady-state and pulsed methods. *Photochem Photobiol* 63:680–685. doi:10.1111/j.1751-1097.1996.tb05673.x
- Frank SN, Bard AJ (1977) Semiconductor electrodes. 12. Photoassisted oxidations and photoelectrosynthesis at polycrystalline titanium dioxide electrodes. *J Am Chem Soc* 99:4667–4675
- Gomathi Devi L, Kavitha R (2014) Review on modified N-TiO₂ for green energy applications under UV/visible light: selected results and reaction mechanisms. *RSC Adv* 4:28265–28299. doi:10.1039/C4RA03291H
- Henle J, Simon P, Frenzel A, Scholz S, Kaskel S (2007) Nanosized BiOX (X= Cl, Br, I) particles synthesized in reverse microemulsions. *Chem Mater* 19:366–373
- Huang R-J et al (2014) High secondary aerosol contribution to particulate pollution during haze events in China. *Nature* 514:218–222
- Huang Y, Wang W, Zhang Q, J-j Cao, R-j Huang, Ho W, Lee SC (2016) In situ fabrication of α -Bi₂O₃/(BiO)₂CO₃ nanoplate heterojunctions with tunable optical property and photocatalytic activity. *Sci Rep* 6:23435. doi:10.1038/srep23435
- Jinlin L et al (2014) Bi₂MoO₆ nanobelts for crystal facet-enhanced photocatalysis. *Small* 10:2791–2795
- Liu B, Fang Y, Li Z, Xu S (2015) Visible-light nanostructured photocatalysts—a review. *J Nanosci Nanotechnol* 15:889–920
- Liu G, Wang L, Yang HG, Cheng H-M, Lu GQM (2010) Titania-based photocatalysts—crystal growth, doping and heterostructuring. *J Mater Chem* 20:831–843
- Long R, Dai Y, Huang B (2009) Structural and electronic properties of iodine-doped anatase and rutile TiO₂. *Comput. Mater. Sci.* 45:223–228
- Marin ML, Santos-Juanes L, Arques A, Amat AM, Miranda MA (2012) Organic photocatalysts for the oxidation of pollutants and model compounds. *Chem Rev* 112:1710–1750
- Martinez Suarez C, Hernández S, Russo N (2015) BiVO₄ as photocatalyst for solar fuels production through water splitting: a short review. *Appl Catal A* 504:158–170. doi:10.1016/j.apcata.2014.11.044
- Sun L et al (2015) Enhanced Visible-light photocatalytic activity of BiOI/BiOCl heterojunctions: key role of crystal facet combination. *ACS Catal* 5:3540–3551. doi:10.1021/cs501631n
- Tada H, Kiyonaga T, S-i Naya (2009) Rational design and applications of highly efficient reaction systems photocatalyzed by noble metal nanoparticle-loaded titanium(IV) dioxide. *Chem Soc Rev* 38:1849–1858. doi:10.1039/B822385H
- Thornalley P, Trotta R, Stern A (1983) Free radical involvement in the oxidate phenomena induced by tert-butyl hydroperoxide in erythrocytes. *BBA-Gen Subj* 759:16–22
- Wang W, Tade MO, Shao Z (2015) Research progress of perovskite materials in photocatalysis- and photovoltaics-related energy conversion and environmental treatment. *Chem Soc Rev* 44:5371–5408. doi:10.1039/C5CS00113G
- Wang Y, Deng K, Zhang L (2011) Visible light photocatalysis of BiOI and its photocatalytic activity enhancement by in situ ionic liquid modification. *J Phy Chem C* 115:14300–14308
- Zhang L, Zhu Y (2012) A review of controllable synthesis and enhancement of performances of bismuth tungstate visible-light-driven photocatalysts. *Catal Sci Technol* 2:694–706. doi:10.1039/C2CY00411A
- Zhang W, Zhang Q, Dong F (2013) Visible-light photocatalytic removal of NO in air over BiOX (X = Cl, Br, I) single-crystal nanoplates prepared at room temperature. *Ind Eng Chem Res* 52:6740–6746. doi:10.1021/ie400615f
- Zhang Y, Sun X, Yang G, Zhu Y, Si H, Zhang J, Li Y (2016) Preparation and characterization of bifunctional BiOCl_xI_y solid solutions with excellent adsorption and photocatalytic abilities for removal of organic dyes. *Mater Sci Semicond Proc* 41:193–199. doi:10.1016/j.mssp.2015.08.040
- Zhao Z, Sun Y, Dong F (2015) Graphitic carbon nitride based nanocomposites: a review. *Nanoscale* 7:15–37. doi:10.1039/C4NR03008G